

# Chloroplasts play a central role in plant defence and are targeted by pathogen effectors

Marta de Torres-Zabala<sup>1</sup>, George Littlejohn<sup>1</sup>, Siddharth Jayaraman<sup>1</sup>, David Studholme<sup>1</sup>, Trevor Bailey<sup>1</sup>, Tracy Lawson<sup>2</sup>, Michael Tillich<sup>3</sup>, Dirk Licht<sup>3</sup>, Bettina Bölter<sup>4</sup>, Laura Delfino<sup>4</sup>, William Truman<sup>5</sup>, John Mansfield<sup>6</sup>, Nicholas Smirnoff<sup>1</sup> and Murray Grant<sup>1\*</sup>

**Microbe associated molecular pattern (MAMP) receptors in plants recognize MAMPs and activate basal defences; however a complete understanding of the molecular and physiological mechanisms conferring immunity remains elusive. Pathogens suppress active defence in plants through the combined action of effector proteins. Here we show that the chloroplast is a key component of early immune responses. MAMP perception triggers the rapid, large-scale suppression of nuclear encoded chloroplast-targeted genes (NECGs). Virulent *Pseudomonas syringae* effectors reprogramme NECG expression in *Arabidopsis*, target the chloroplast and inhibit photosynthetic CO<sub>2</sub> assimilation through disruption of photosystem II. This activity prevents a chloroplastic reactive oxygen burst. These physiological changes precede bacterial multiplication and coincide with pathogen-induced abscisic acid (ABA) accumulation. MAMP pretreatment protects chloroplasts from effector manipulation, whereas application of ABA or the herbicide DCMU inhibits the MAMP-induced chloroplastic reactive oxygen burst, and enhances growth of a *P. syringae* *hrpA* mutant that fails to secrete effectors.**

## 1 Introduction

In plants MAMP-triggered immunity (MTI) provides broad-spectrum protection against a diverse range of potential pathogens. This is achieved through the deployment of a range of surface exposed and cytosolic pattern recognition receptors to detect the presence of potentially pathogenic microbes and activate defence. Successful pathogens attenuate these sophisticated surveillance systems and downstream defences through the collective actions of ‘effector’ molecules<sup>1,2</sup>. Understanding how the effectors collaborate to cause disease will provide a framework allowing the design of targeted intervention strategies through the rewiring of defence networks to nullify pathogen virulence.

Knowledge of the downstream signalling networks targeted by pathogens, and specifically, the physiological outcomes of these responses, is limited. Chloroplasts play a central role in integrating multiple environmental stimuli<sup>3</sup> and accommodate many biosynthetic pathways, including those for plant hormones. A common strategy deployed by pathogens to hijack host immune signalling is to alter the phytohormone balance. Chloroplasts also produce reactive oxygen species (ROS) that are potentially damaging but which also act as signalling molecules<sup>4</sup> and may have a direct antimicrobial role. Considering the importance of ROS and hormone balance to plant–pathogen interactions<sup>5,6</sup>, the chloroplast represents a prime target for manipulation by pathogens.

Understanding the physiological processes targeted by effectors is challenging, not least due to redundancy and cooperativity in pathogen effector repertoires. The hemi-biotroph *Pseudomonas syringae* pv. *tomato* strain DC3000 (DC3000) delivers ~28 type III effector proteins (T3E) into plants via a type III secretion system (T3SS)<sup>7</sup>. To understand the early events underlying DC3000 virulence strategies we analysed high-resolution time course microarray data from leaves challenged with DC3000 or the disarmed *hrpA* mutant, which is unable to produce a functional T3SS.

## Results

Focusing on the expression of nuclear encoded chloroplast genes (NECGs; Fig. 1a), our data confirmed previously reported changes in the NECG transcriptome in response to syringe infiltration of both the wild-type and *hrpA* mutant bacteria<sup>8</sup>, consistent with a conserved plants response to MAMPs. Strikingly, within 2 hpi of bacterial challenge, ~10% of the 3,678 NECGs (comprising ~14% of the genome) were significantly differentially (SD) induced, and between 15% and 20% SD suppressed (as determined using the Bioconductor package LIMMA<sup>9</sup> using the Benjamini–Hochberg false discovery rate correction and 0.05 *P* value cut-off; for summary statistics see Supplementary Table 1). By 4 hpi, NECGs were strongly over-represented, accounting for ~30% of all SD suppressed genes. Notably, transcripts encoding photosynthesis-related processes were suppressed after DC3000 or *hrpA* challenges, whereas some transcripts involved in chorismate, tryptophan and JA biosynthesis were SD induced (Supplementary Fig. 1a). Consistent with the former finding, challenge with the flagellin MAMP peptide, flg22 (ref. 10), or the necrotroph *Botrytis cinerea*<sup>11</sup> also suppresses photosynthesis-related transcripts (Supplementary Fig. 1b). Yet, despite the over-representation of NECGs, clear differences between bacterial challenges were evident 3 hpi (Fig. 1a, DC3000 vs *hrpA*) coinciding with the delivery of DC3000 effectors.

The dynamics of SD-regulated NECGs relative to mock challenge are captured by representative scatter plots in Fig. 1b. In these plots red represents NECGs SD regulated between wild-type DC3000 and mock MgCl<sub>2</sub> challenge, and blue NECGs SD regulated between *hrpA* mutant and mock. Note that red and blue denote SD-regulated NECGs in response to *hrpA* or wild-type challenge compared to mock but not in both. Green represents NECGs SD changing in both wild-type and *hrpA* challenge, compared with mock inoculation, thus representing MAMP response genes not modified by effectors. To clarify, the differential expression observed represents:

<sup>1</sup>Biosciences, College of Life and Environment Sciences, University of Exeter, Exeter EX4 4QD, UK. <sup>2</sup>School of Biological Sciences, University of Essex, Colchester CO4 3SQ, UK. <sup>3</sup>Max Planck Institute of Molecular Plant Physiology, Am Mühlenberg 1, Potsdam-Golm D-14476, Germany. <sup>4</sup>Department of Biology I, Botany, Ludwig-Maximilians-Universität München, Großhaderner Strasse 2–4, Planegg-Martinsried D-82152, Germany. <sup>5</sup>Department of Plant Biology, University of Minnesota, USA. <sup>6</sup>Department of Life Sciences, Imperial College, London, UK. \*e-mail: m.r.grant@exeter.ac.uk

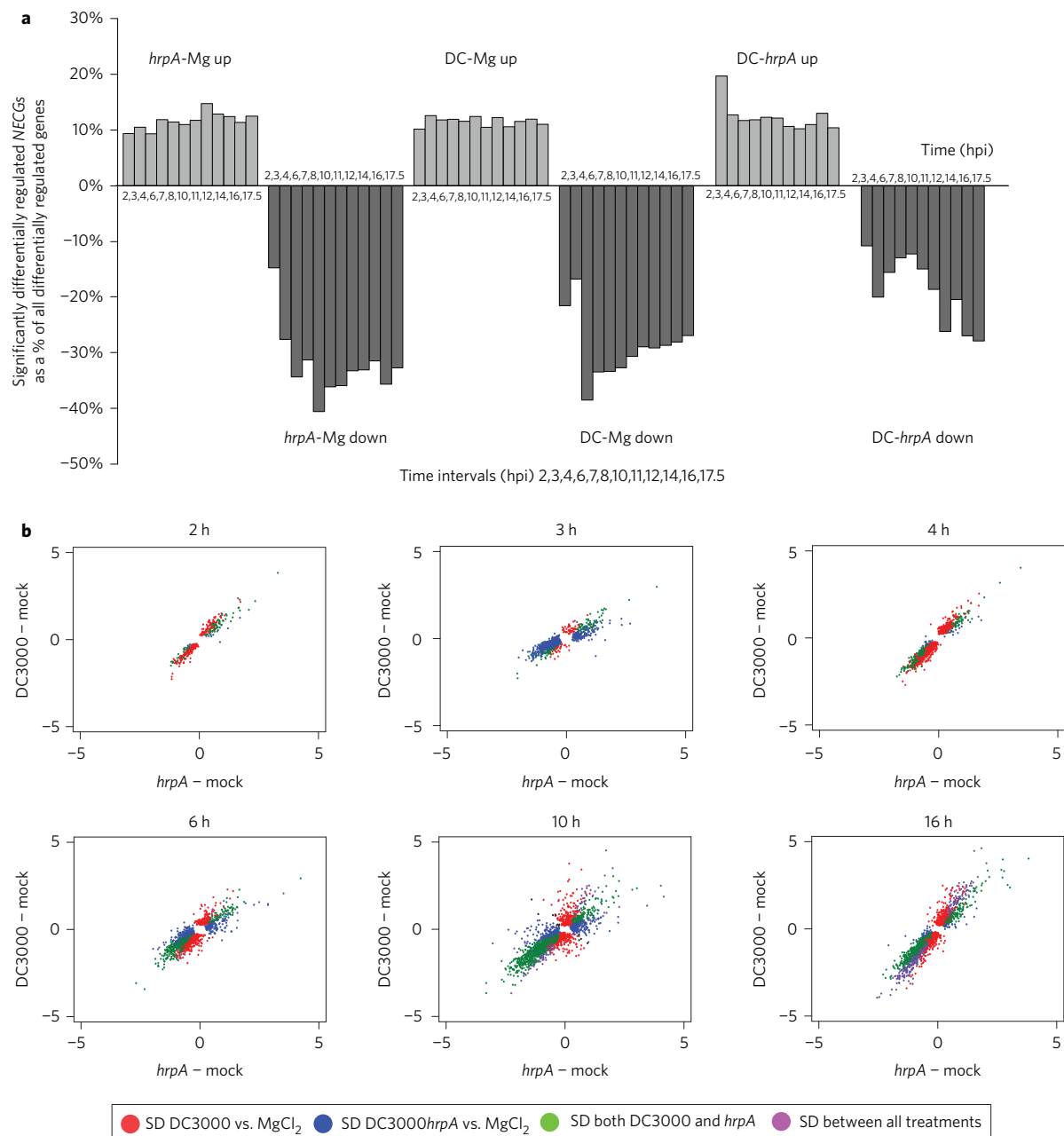


**Figure 1 | Nuclear encoded chloroplast transcripts dynamics in defence and disease responses to *Pseudomonas syringae* pv. tomato DC3000.**

**a**, Representation of significantly up- or downregulated NECGs relative to all SD regulated genes. NECGs represent ~14% of the transcriptome. **b**, Dynamics of NECG expression represented graphically at each time point as a scatter plot. Red represents genes SD in expression between wild-type DC3000 and mock ( $\text{MgCl}_2$ ) challenge, and blue SD between *hrpA* mutant and mock. Note that red and blue denote genes SD in response to wild-type or *hrpA* challenges, respectively, but not both. Green describes genes with SD expression in both wild-type and *hrpA* challenges, compared with mock inoculation (MAMP responsive). Violet represents genes SD between all three treatments. The 3,678 NECG annotations were derived from the TAIR9 release. Genes SD expressed between treatments was determined using the Bioconductor package LIMMA using the Benjamini–Hochberg false discovery rate correction and a *P* value cut-off of 0.05.

1 red, effector induced changes; blue, MAMP modified by effectors;  
2 green, persistent MAMP responses and violet, captures NECDs  
3 SD regulated between all three treatments (these appear late in the  
4 time course).

5 By 2 hpi a common MAMP response (green) is seen. Already  
6 effector modulation of NECGs by DC3000 challenge compared to  
7 mock is evident (red profile). However, there are not yet significant  
8 differences between DC3000 and *hrpA* treatments (no SD-regulated  
9 genes 2 hpi in the DC-*hrpA* analysis, Fig. 1a and Supplementary  
10 Table 1). These profiles are capturing the earliest transcriptional

reprogramming events resulting from T3E delivery between ~1.5  
and 2 hpi (ref. 12), where gene dynamics have not yet diverged  
from the basal MAMP signature. By 3 hpi, effector activity is  
clearly evident, with the slope of the plot and the abundant blue sig-  
nature indicating that T3Es are beginning to override general  
MAMP responses. The highly dynamic and transient nature of  
this early transcriptional response is illustrated by a marked  
change in the NECG signature at 4 hpi, with pronounced red and  
green profiles. By 6 hpi there is clear impact of T3Es on MAMP  
regulated genes, reflected by an increasing density and amplitude 20

1 of red signals. Genes markedly different between all treatments  
 2 (violet) increase from a minor component 6 hpi to represent a  
 3 major proportion of SD genes 16 hpi. Notably, MAMP-induced  
 4 responses (green) are still abundant 16 hpi, reinforcing continuous  
 5 transcriptional regulation of NECGs throughout the expression of  
 6 defence. In summary, NECGs are highly represented amongst SD  
 7 expressed genes between mock and either *hrpA* mutant or virulent  
 8 wild-type DC3000. Effectors modify the MAMP signature as early  
 9 as 2 hpi, with NECGs SD regulated by T3Es measurable within 3  
 10 hpi. Effectors act to both enhance and suppress gene expression  
 11 caused by MAMPs and impose a transcriptome representing suc-  
 12 cessful establishment of disease, a large proportion of which com-  
 13 prises NECGs (Supplementary Table 1 and Fig. 1a).

14 The strong and early suppression of photosynthesis-related tran-  
 15 scription after both challenges is consistent with photosynthetic pro-  
 16 cesses being targeted by MAMPs (Supplementary Fig. 1). To  
 17 explore the physiological impacts of the observed dynamic  
 18 changes in NECG expression we recorded net photosynthetic  
 19 CO<sub>2</sub> assimilation ( $A_{\text{sat}}$ ) following inoculation. Strikingly, DC3000  
 20 but not *hrpA* challenged leaves showed a decrease in assimilation  
 21 between 6 and 8 hpi (Fig. 2a). Unexpectedly,  $A/C_i$  curves (reporting  
 22 photosynthesis versus intercellular CO<sub>2</sub>) showed that photosyn-  
 23 thesis is not restored by high intercellular CO<sub>2</sub> (Fig. 2b). Thus sto-  
 24 matal closure would not simply explain the DC3000-induced  
 25 suppression of CO<sub>2</sub> assimilation. The rapid suppression of photo-  
 26 synthesis represents one of the earliest physiological responses  
 27 detected to DC3000. We used chlorophyll fluorescence imaging  
 28 to further investigate the mechanism of DC3000 action.  
 29 Challenge with DC3000 but not *hrpA* or mock inoculation  
 30 caused a rapid decrease in maximum dark-adapted quantum effi-  
 31 ciency ( $Fv/Fm$ ; Fig. 2c,i), maximum operating efficiency of photo-  
 32 system II (PSII) photochemistry at a given light intensity if all the  
 33 PSII centres are oxidized ( $Fv'/Fm'$ , Fig. 2d) and the efficiency  
 34 with which light absorbed by PSII is used for  $Q_A$  reduction and  
 35 linear electron transport at a given light intensity ( $Fq'/Fm'$ ;  
 36 Fig. 2e).  $q_L$  also increased by 6 hpi with DC3000 but not *hrpA*  
 37 (Fig. 2f).  $q_L$  estimates the fraction of open PSII centres and the ox-  
 38 idation state of the primary PSII quinone acceptor ( $Q_A$ , ref. 13),  
 39 indicating that the  $Q_A$  is more oxidized and suggesting decreased  
 40 electron transport from PSII. Non-photochemical quenching  
 41 (NPQ) increased transiently at 4–10 hpi (Fig. 2g,i). Elevated  
 42 NPQ indicates increased excitation energy dissipation as heat,  
 43 caused either by proton gradient-dependent processes involving  
 44 PsbS and xanthophylls (energy-dependent quenching), or  
 45 photoinhibitory quenching<sup>14</sup>.

46 Inhibition of photosynthesis by a biotrophic pathogen is poten-  
 47 tially counter-intuitive, because it would reduce sugars available  
 48 to the pathogen. We verified the effect by recording <sup>14</sup>CO<sub>2</sub> assimi-  
 49 lation. After 10 h, leaves inoculated with DC3000 fixed less <sup>14</sup>CO<sub>2</sub>  
 50 than mock or *hrpA*-inoculated leaves (Supplementary Fig. 2a)  
 51 whereas the neighbouring uninoculated leaves were unaffected  
 52 (Supplementary Fig. 2b). DC3000 would not lack fixed <sup>14</sup>C presum-  
 53 ably because it would be translocated from the neighbouring leaves,  
 54 thereby providing carbon sources for the pathogen.

55 Our data are consistent with rapid T3E inactivation of PSII,  
 56 resulting in decreased electron transport and non-stomatal inhi-  
 57 bition of CO<sub>2</sub> assimilation. While decreases in transcript abundance  
 58 of NECGs have been observed<sup>8,11,15,16</sup>, they have not previously been  
 59 linked to changes in photosynthetic metabolism. Critically, the T3E-  
 60 induced changes in chloroplast physiology are initiated prior to  
 61 rapid bacterial multiplication which occurs only after a period of  
 62 6–8 h of bacteriostasis in the intercellular space, during which the  
 63 dynamic exchange of MAMP signals and effectors takes place  
 64 (Fig. 2h)<sup>17</sup>. T3E inactivation of PSII is not specific to DC3000,  
 65 both *Ps* pv. *maculicola* M4 (ref. 18) and *Xanthomonas campestris*  
 66 pv. *campestris* (Xcc) race 6 (ref. 19) also suppressed  $Fv/Fm$ , but

this effect occurred later and was weaker, correlating with their  
 reduced virulence in *Arabidopsis* (Supplementary Fig. 3).

We further explored the surprising finding that, despite suppress-  
 ing a significant proportion of NECGs (Supplementary Table 1 and  
 Fig. 1) photosynthesis was unaffected in *hrpA* challenged leaves  
 (Fig. 2a). Remarkably, DC3000 suppression of  $Fv/Fm$  was prevented  
 in leaves pretreated 24 h previously with flg22 (1 μM) but not SA  
 (1 mM) (Fig. 3a and Supplementary Fig. 4a). Non-pathogenic  
*P. fluorescens* did not affect  $Fv/Fm$  and CUCPB6032 (ref. 20), a  
 reduced virulence DC3000 strain, had less effect on  $Fv/Fm$  than  
 DC3000 (Fig. 3b and Supplementary Fig. 4b). By contrast, the *fliC*  
 mutant, which lacks bacterial flagellin<sup>21</sup>, elicited a much stronger  
 reduction in  $Fv/Fm$  compared to DC3000, indicating that flagellin  
 perception plays an important role in the maintenance of photosyn-  
 thetic capability (Fig. 3b and Supplementary Fig. 4b). Pretreatment  
 of the MAMP receptor mutant *fls2-2* (ref. 22) with flg22 failed to  
 prevent DC3000 suppression of  $Fv/Fm$ , whereas activation of the  
 bacterial elongation factor thermo unstable (EF-Tu) receptor by  
 elf18 MAMP peptide<sup>23</sup> protects the chloroplast in the *fls2* back-  
 ground (Fig. 3c and Supplementary Fig. 4c). Correspondingly, the  
 hypersusceptible *eds1* mutant, which compromises MAMP and  
 effector triggered immunity<sup>24</sup> displayed markedly enhanced sup-  
 pression of  $Fv/Fm$  (Supplementary Fig. 4d). The protection of the  
 chloroplast from effector-mediated perturbations has emerged as  
 an important and unexpected component of MTI.

Effectors delivered by DC3000 induce rapid increases in ABA  
 within 6 hpi and pretreatment with ABA enhances susceptibility  
 to DC3000 (ref. 17). It was therefore important to determine  
 whether ABA homeostasis influenced photosynthesis. Co-infiltra-  
 tion of DC3000 with ABA increased NPQ (Supplementary  
 Fig. 4e) and decreased  $Fv/Fm$  (Fig. 3d and Supplementary Fig. 5a)  
 compared with DC3000 alone. Importantly, neither ABA alone  
 nor co-infiltration with *hrpA* affected  $Fv/Fm$ . ABA pretreatment  
 also induced larger decreases in  $Fv/Fm$  following challenge with  
 100 *PsmM4*, or two virulent races of *Xcc* (Fig. 3e and Supplementary  
 Fig. 5b). *Arabidopsis* ABA hypersensitive protein phosphatase 2C  
 (PP2C) mutants are more susceptible to DC3000 (ref. 25) whereas  
 the ABA deficient *Arabidopsis aldehyde oxidase 3* (*aoa3*) mutant  
 is more resistant to DC3000 infection<sup>17</sup>. DC3000 challenged PP2C  
 triple mutant *abi1/abi2/hab1* (*triple*)<sup>26</sup> showed significantly faster  
 and stronger suppression of  $Fv/Fm$  compared to Col-0, whereas  
 107  $Fv/Fm$  in the *aoa3* mutant was less affected by DC3000 challenge  
 compared to wild-type Col-0 (Supplementary Fig. 5d). Therefore  
 effector perception rapidly modifies ABA signalling, which directly  
 impacts on photosynthesis during the critical first few hours after  
 bacterial challenge.

To link chlorophyll fluorescence dynamics with suppression of  
 basal defence we first monitored luciferase activity of a transgenic  
 line expressing *FLS2 induced receptor kinase 1* (*FRK1*)<sup>27</sup> fused to  
 luciferase (Fig. 3g). The construct reports activation of FLS2. The  
 suppression of luciferase activity between 2 and 4 hpi DC3000  
 was found to correlate with specific changes in NECG expression  
 (Fig. 1) and is coincident with suppression of photosynthesis  
 (Fig. 2). Notably, all these transcriptional changes occur before  
 rapid bacterial multiplication 8 hpi. Secondly we found that the  
 hypersensitive *triple* PP2C mutant showed strikingly rapid suppres-  
 sion of  $Fv/Fm$ , which was phenocopied by exogenous application of  
 123 10 μM ABA, whereas  $Fv/Fm$  was only mildly reduced in DC3000  
 challenged *aoa3* leaves (Fig. 3g). In summary, Fig. 3a–c links  
 124  $Fv/Fm$  to suppression of MTI, showing that flg22 but, surprisingly,  
 not SA (which is not synthesized until significantly later in the infec-  
 125 tion process<sup>17</sup>) prevents T3E suppression of  $Fv/Fm$  whereas *fliC*  
 mutant challenge enhanced  $Fv/Fm$  suppression. Figure 3d–f illus-  
 126 trates the importance of pathogen-induced ABA in suppression of  
 127  $Fv/Fm$ . These panels show that (i) effectors have to be delivered  
 128 and that (ii) virulent bacteria produce ABA to suppress  $Fv/Fm$

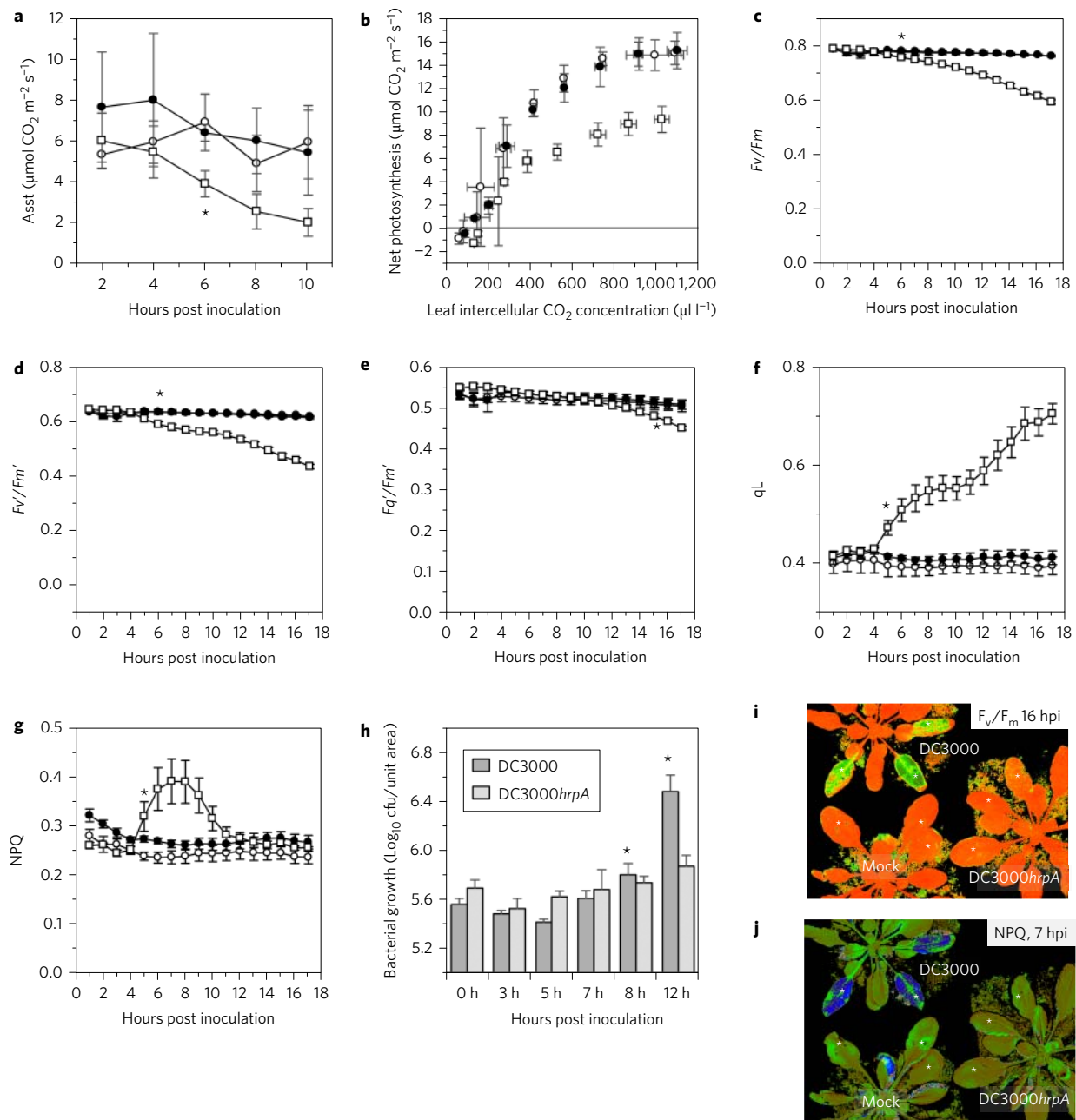


**Figure 2 | *Pseudomonas syringae* DC3000 rapidly inhibits photosynthesis in *Arabidopsis thaliana*.** For all panels, mock – open circle, DC3000*hrpA* – closed circles, DC3000 – open squares. **a**, DC3000 decreases photosynthetic  $\text{CO}_2$  assimilation in saturating light ( $A_{sat}$ ). **b**,  $A/C_i$  curve showing the relationship between photosynthesis ( $A$ ) and intercellular  $\text{CO}_2$  concentration ( $C_i$ ) at 10 hpi. **c**, Maximum quantum efficiency of PSII ( $F_v/F_m$ ), **d**, maximum light adapted quantum efficiency of PSII ( $F_v'/F_m'$ ) and **e**, PSII operating efficiency ( $F_q'/F_m'$ ) are decreased by DC3000 challenge and **f**, photochemical quenching of PSII (qL) is increased. **g**, NPQ transiently increases 4 hpi after DC3000 inoculation. **h**, DC3000 bacterial growth (inoculum of  $\sim 0.5 \times 10^8$  cfu  $\text{ml}^{-1}$ ) is restricted until 8 hpi. Asterisks show significant differences in bacterial growth ( $t$ -test,  $P < 0.05$ ) from time 0 (mean  $\pm$  SD;  $n = 6$ ). **i**, False colour image of  $F_v/F_m$  at 16 hpi showing a decrease (green/yellow) after DC3000 challenge. Asterisks show inoculated leaves. **j**, False colour image of NPQ at 7 hpi showing the increase (blue) after DC3000 challenge. Asterisks show inoculated leaves. Photosynthesis values (**a**) are means  $\pm$  SD ( $n = 4$ ), and show that DC3000 differs significantly from DC3000*hrpA* and mock treatments from 8 hpi ( $*P < 0.001$ ; two-way ANOVA). Chlorophyll fluorescence parameters (**c–g**) are means  $\pm$  SD (mock and *hrpA*,  $n = 3$ ; DC3000,  $n = 4$ ). ANOVA with the least significant difference *post hoc* test and Bonferroni multiple comparison correction shows that DC3000 differs significantly from DC3000*hrpA* and mock treatments for all time points at and beyond the asterisk ( $P < 0.05$ ).

1 prior to bacterial multiplication. Additionally, Fig. 3f provides the  
 2 temporal context, linking suppression of basal immunity to  
 3 reduced  $F_v/F_m$  and the important role of pathogen-induced ABA  
 4 in this process. We conclude that inhibition of photosynthesis is a  
 5 prerequisite for suppression of MTI leading to bacterial multipli-  
 6 cation (Fig. 1j) and that these effects are underpinned by modu-  
 7 lation of ABA signalling.

Effectors induce transcriptional changes in NECGs but the rapid  
 suppression of NPQ and  $F_v/F_m$  also suggested the possibility of  
 their direct action in the chloroplast. The *P. syringae* effectors,  
 HopI1, HopN1 and AvrRps4/HopK, have been localized to the  
 chloroplast<sup>28–32</sup>. Notably, AvrRps4 and HopK use non-canonical  
 import sequences<sup>30</sup> suggesting effectors have evolved multiple strat-  
 egies to localize to chloroplasts. HopN1, a cysteine protease, 14

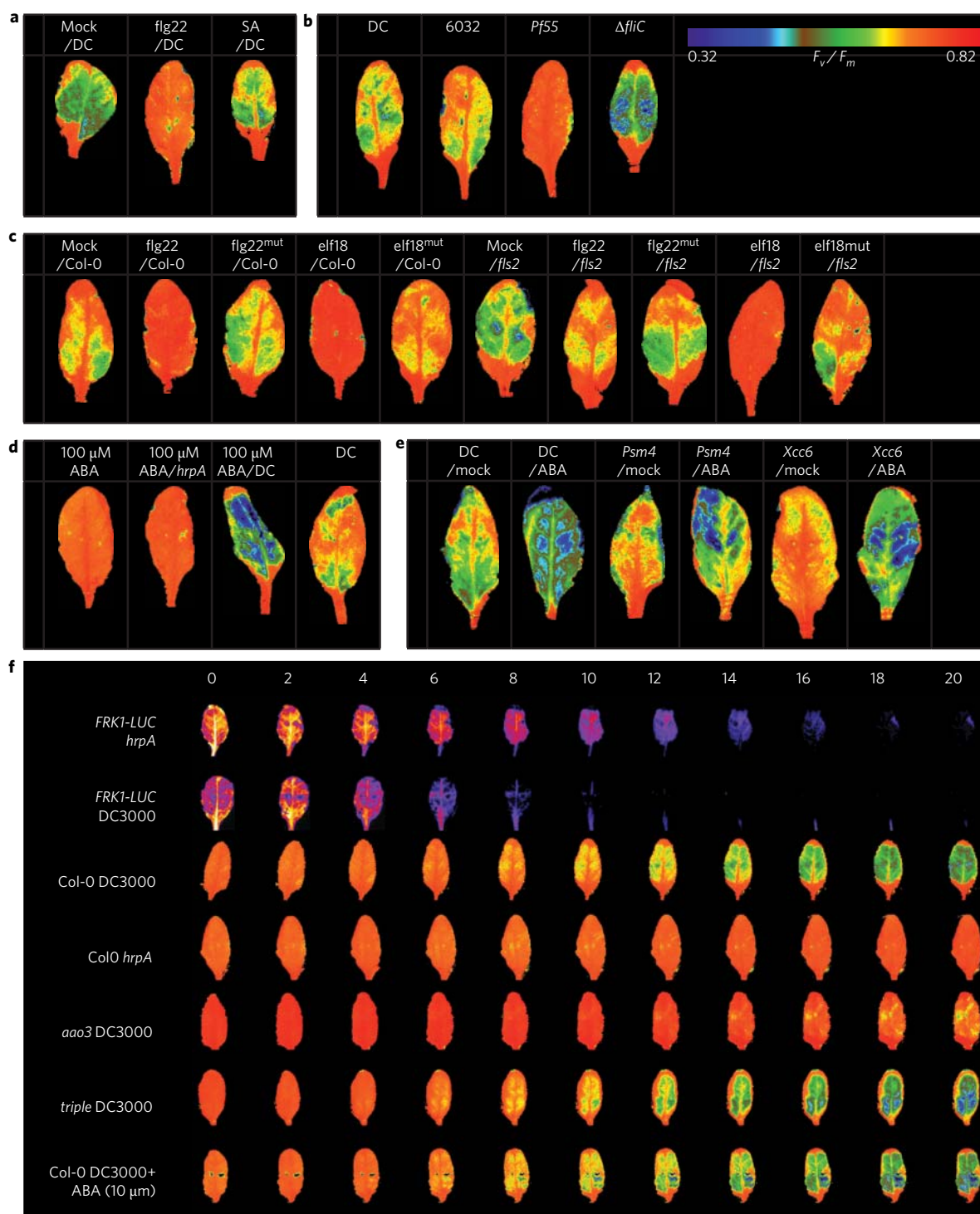


**Figure 3 | DC3000 effectors suppress  $F_v/F_m$  in an ABA dependent manner. a–e**  $F_v/F_m$  in single leaves of representative treatments at 18 hpi, and **f**, representative leaves across a treatment time course. See Supplementary Figs 4 and 5 for quantitative data and whole plant images. MAMP pretreatment attenuates *P. syringae* suppression of  $F_v/F_m$ . **a**, Pretreatment 24 hpi with flagellin peptide (flg22; 1  $\mu$ M) but not SA (1 mM), prevents DC3000 suppression of  $F_v/F_m$ . **b**, MAMPs restrict T3E mediated  $F_v/F_m$  suppression. Representative Col-0 leaves challenged with non-pathogenic *Pseudomonas fluorescens* (Pf55) containing a functional T3SS, CUCPB6032 a minimally virulent DC3000 derivative, DC3000 or  $\Delta fliC$  which lacks bacterial flagella<sup>20,21</sup>. A strong reduction in  $F_v/F_m$  (18 hpi) elicited by the *fliC* mutant reflects the importance of MAMPs in chloroplast mediated MTI. **c**, Col-0 or *fls2-2* mutant leaves mock treated or challenged with flg22, elf18, or their respective mutant non-binding ligands, flg22-tu or elf18<sup>mut</sup> (all at 1  $\mu$ M). After 24 h, leaves were challenged with DC3000. **d**, T3E suppression of  $F_v/F_m$  is enhanced by ABA. Col-0 leaves challenged with ABA alone, or co-infiltrated with either *hrpA* or DC3000 at 100  $\mu$ M (see Supplementary Fig. 4e (NPQ) and 5a ( $F_v/F_m$ ) for additional concentrations). **e**, ABA enhances suppression of  $F_v/F_m$  by *P. maculicola* M4 (*Psm4*) or *X. campestris* pv. *campestris* (*Xcc*) race 6 (see Supplementary Fig. 5B for *Xcc* race 1). **f**, Summary of  $F_v/F_m$  responses. Hourly measurements of  $F_v/F_m$  in DC3000 challenged leaves of wild-type (Col-0), the hypersensitive *triple* and ABA deficient *aao3* mutants or following co-infiltration with ABA (10  $\mu$ M) compared DC3000/*hrpA* challenge (see Supplementary Fig. 5c for additional ABA mutant data). A reporter line expressing *flagellin induced receptor kinase 1* (*FRK1*) fused to luciferase was used to monitor suppression of basal defence by DC3000. All bacterial treatments were at  $\sim 0.5 \times 10^8$  S ml<sup>-1</sup>.

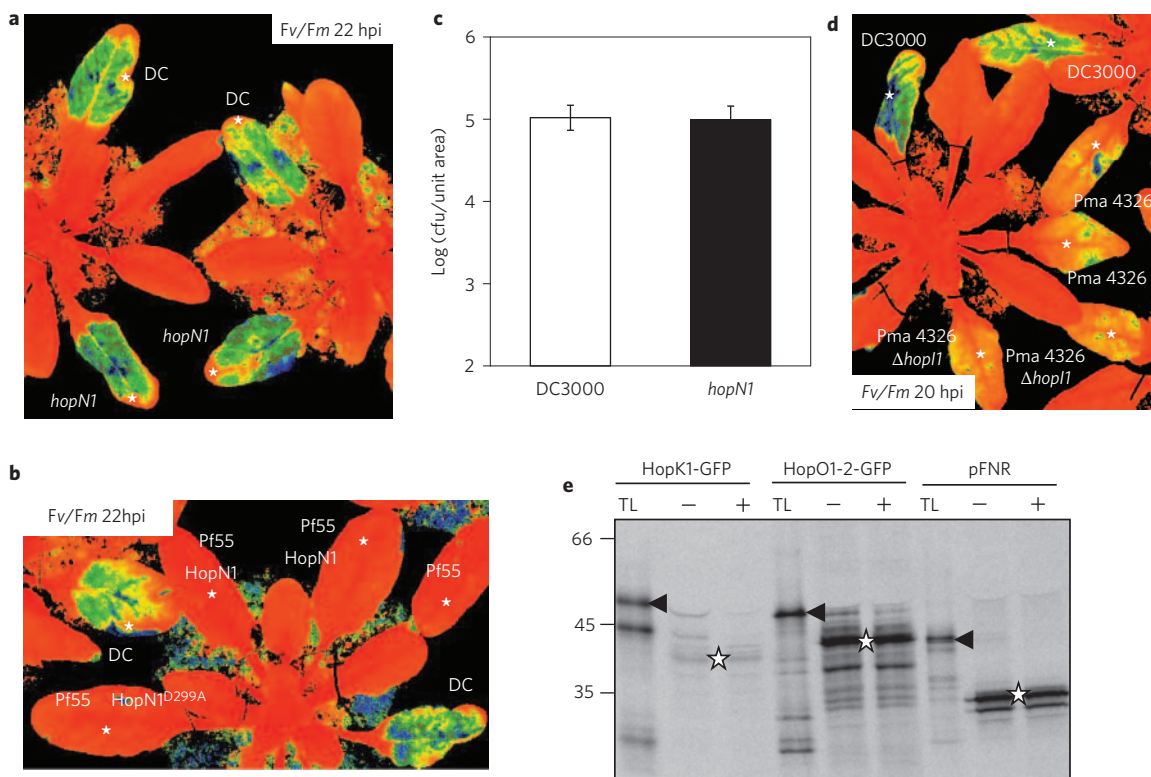


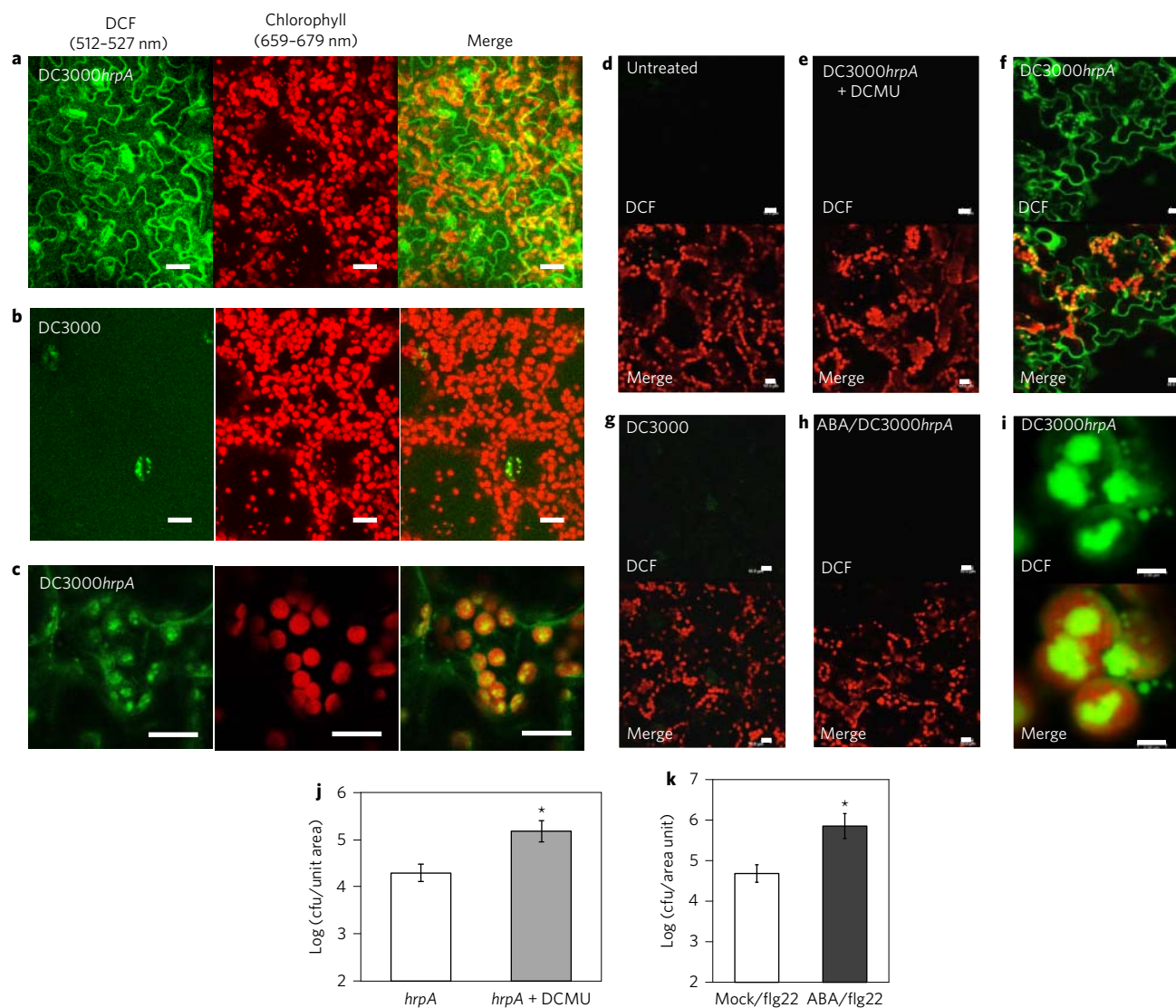
**Figure 4 | Chloroplast localized HopN1 and HopI do not modify *Fv/Fm*.** **a, b**, Neither deletion of HopN1 nor delivery of HopN1, or its catalytic derivative HopN1<sup>D229A</sup>, modified *Fv/Fm*. **c**, Deletion of HopN1 does not affect susceptibility to DC3000. Bacterial growth in *hopN1* 4 dpi with DC3000 ( $\sim 0.5 \times 10^5$  cfu ml<sup>-1</sup>; mean,  $n = 6$ , error SD  $\pm 1$ ). **d**, Deletion of HopI does not impact *Fv/Fm*. **e**, The N-terminus of HopO1-2 is imported into chloroplasts. The import of effector N-termini ( $\sim 150$  aa fused to GFP) into pea chloroplasts was analysed using *in vitro* transcription/translation assays and visualized by <sup>35</sup>S-autoradiography. The previously validated HopK (control effector), the putative effector ribosyltransferase, HopO1-2 and an import control (pFNR; precursor of the chloroplast-targeted ferredoxin-NADP(+) oxidoreductase) were transported into isolated pea chloroplasts. Their putative mature forms (labelled by asterisks) but not their precursors (arrowheads) are resistant to thermolysin treatment. TL: 10% of translation product used for import experiments, ±: import reactions with and without thermolysin treatment.

1 specifically targets and proteolytically cleaves tomato PsbQ (ref. 31),  
 2 an extrinsic protein of PSII. In *Nicotiana benthamiana* HopN1  
 3 reduced early immunity responses, altered electron transport and  
 4 suppressed ROS production<sup>31</sup>. However, we found that neither  
 5 DC3000Δ*HopN1* nor delivery of HopN1 or its catalytically inactive  
 6 HopN1<sup>D299A</sup> derivative by *P. fluorescens* altered *Fv/Fm* or reduced  
 7 virulence on *Arabidopsis* (Fig. 4a–c). Similarly HopI, which mod-  
 8 ifies thylakoid structure, suppresses salicylic acid accumulation and  
 9 targets HSP70, did not alter *Fv/Fm* (Fig. 4d)<sup>32</sup>. These data suggest  
 10 multiple effectors may cooperate to alter PSII function.

11 To explore organelle targeting more fully, we analysed a core set  
 12 of 48 *Pseudomonas* effector proteins (derived from www.effector.  
 13 org) with ChloroP (ref. 33) and identified 21 possible chloroplast-  
 14 targeted effectors, including the experimentally validated HopK1  
 15 and HopN1 (Supplementary Table 2). Using serine frequency scan-  
 16 ning to compare the 28 effectors with known plant chloroplast local-  
 17 ized proteins confirmed a potential chloroplast location for 21 of  
 18 the effectors (Supplementary Fig. 6). ChloroP predicted potential  
 19 chloroplast targeting sequences in putative effectors from a range  
 20 of other sequenced bacterial genomes, including 54% of the 28  
 21 DC3000 effectors and 53% of the 19 *Xcc* effectors (Supplementary  
 22 Table 3). Further evidence that effectors target the chloroplast was  
 23 derived from the yeast two hybrid interaction data of plant pathogen  
 24 effectors against  $\sim 8,000$  *Arabidopsis* proteins<sup>34</sup>. An interaction  
 25 network generated for *P. syringae* effectors predicted a number of  
 26 T3Es (e.g. HopR1, HopBB1, HopZ) that can interact with multiple  
 27 chloroplast proteins. These chloroplast predicted proteins them-  
 28 selves interact with two or more effectors (Supplementary

Fig. 7a). Thus sequence unrelated effectors are potentially chloro- 29  
 plast localized and have common potential susceptibility targets, 30  
 consistent with redundancy and robustness in virulence strategies. 31

Based on these data we tested whether the N-termini ( $\sim 150$  aa) 32  
 of a set of the putatively chloroplast localized effectors are imported 33  
 in chloroplast import assays<sup>35</sup>. We chose HopR1 because it is a 34  
 widely distributed T3E in proteobacterial phytopathogens<sup>36</sup>, and 35  
 HopO1-2 because it has predicted ADP-ribosyl-transferase activity, 36  
 similar to HopU1, that ribosylates at least three chloroplast RNA- 37  
 binding proteins *in vitro*, although there is no evidence that 38  
 HopU1 localizes to the chloroplast<sup>37</sup>. We found that *in vitro* trans- 39  
 lated HopO1-2 was efficiently imported into isolated pea chloro- 40  
 plast (Fig. 4e). HopO1-2 is predicted to interact with one plastid 41  
 localized protein (At3g07780). HopR1 was also imported to chloro- 42  
 plast (Supplementary Fig. 7b,c). Four independent effectors are 43  
 predicted to interact with one or more of HopR1's targets, and 44  
 AvrPto and HopBB1 share HopR1's chloroplast targets 45  
 (Supplementary Fig. 7a). Notably, the chloroplast target of HopR1 46  
 (and HopBB1), PTF1/TCP13 (PLASTID TRANSCRIPTION 47  
 FACTOR 1/TEOSINTE BRANCHED1, CYCLOIDEA AND PCF 48  
 TRANSCRIPTION FACTOR 13) is a transcription factor that 49  
 binds to the promoter of *psbD* (ref. 38). *psbD* encodes the PSII 50  
 reaction centre protein D2, which along with D1 (PsbA) bind all the 51  
 redox-active cofactors involved in the energy conversion process<sup>39</sup>. 52  
 Loss of D2 blocks electron transport, resulting in destabilization 53  
 of the PSII complex<sup>40</sup>. TCP13 loss of function plants are more resist- 54  
 ant to DC3000 but more susceptible to *Golovinomyces orontii* and 55  
*Hyaloperonospora arabidopsidis*<sup>41</sup>. 56



1 The generation of apoplastic ROS is a hallmark of MTT<sup>42</sup>.  
 2 Photosynthesis is also a potential source of ROS in basal defence.  
 3 We hypothesized that suppression of photosynthesis-derived ROS  
 4 may be a specific mechanism to attenuate basal defence. We exam-  
 5 ined ROS production after apoplastic ROS generation<sup>43</sup> and prior to  
 6 bacterial multiplication using the probe 2',7'-dichlorodihydrofluor-  
 7 escein diacetate (H<sub>2</sub>DCF-DA, ref. 44). Strikingly, by 5 hpi, a  
 8 strong increase in oxidized dichlorofluorescein (DCF) signal was  
 9 detected by confocal microscopy in *hrpA* (Fig. 5a,c,f,i) but not  
 10 DC3000 challenged leaf cells (Fig. 5b,g) or mock inoculated tissue  
 11 (Fig. 5d). Although the probe is diffusible after hydrolysis or oxida-  
 12 tion, a strong oxidized DCF signal was clearly seen in individual  
 13 chloroplasts (Fig. 5c,i). H<sub>2</sub>DCF-DA is sensitive to H<sub>2</sub>O<sub>2</sub> but is not  
 14 specific<sup>45</sup>. Blocking electron transport from PSII with 3-(3,4-  
 15 dichlorophenyl)-1,1-dimethylurea (DCMU) has previously been

shown to inhibit the production of H<sub>2</sub>O<sub>2</sub> by oxygen photoreduction 16  
 at PSI<sup>46</sup> and to increase singlet oxygen production by PSII<sup>47</sup>. DCMU 17  
 co-infiltration (10  $\mu$ M) abolished the *hrpA*-induced probe oxida- 18  
 tion, consistent with photosynthetic production of H<sub>2</sub>O<sub>2</sub> or 19  
 another oxidant derived from it (Fig. 5e). We conclude that the 20  
 effector-dependent inhibition of photosynthetic electron transport 21  
 decreases MAMP-induced photosynthetic hydrogen peroxide produc- 22  
 tion. To explore the link between photosynthetic ROS produc- 23  
 tion and bacterial growth we co-infiltrated Arabidopsis leaves 24  
 with *hrpA* and DCMU. Remarkably, DCMU treatment not only 25  
 abolished the induction of ROS by *hrpA* challenge (Fig. 5j), but 26  
 also significantly enhanced growth of *hrpA*, suggesting that inhi- 27  
 bition of photosynthesis and consequent restriction of chloro- 28  
 plast-sourced ROS production is required for full immunity 29  
 (Fig. 5d). ABA pretreatment enhances growth of *hrpA* (ref. 25). 30

1 Consistently, ABA pretreatment prior to *hrpA* challenge also abol-  
 2 ished ROS production (Fig. 5h) and ABA pretreatment of leaves  
 3 24 h prior to flg22 treatment also prevented flg22-mediated restric-  
 4 tion of DC3000 growth (Fig. 5k).

5 PSII disruption is also associated with singlet oxygen pro-  
 6 duction<sup>48</sup>. Publically available microarray data revealed that the  
 7 DC3000 NECG signature was remarkably similar to those resulting  
 8 from treatments (lincomycin, norflurazon) and mutants (*flu1*)  
 9 which cause singlet oxygen formation (Supplementary Fig. 8).  
 10 However, these sampling times are considerably later than the  
 11 chloroplast ROS generation and coincide with exponential bacterial  
 12 growth. As neither *executer* single or double mutant suppressors of  
 13 *flu1* (*ex1/ex2*, ref. 49) showed altered susceptibility to DC3000  
 14 (Supplementary Fig. 9a) we conclude that these signatures are a  
 15 late response to infection. Moreover, the classical *genome uncoupled*  
 16 mutants<sup>50</sup> *gun4*, *gun5/abar-2* (which are largely responsible for the  
 17 singlet oxygen signature in Supplementary Fig. 8) and *gun1*, all  
 18 exhibited wild-type susceptibility (Supplementary Fig. 9b,c). Thus  
 19 a different mechanism of inter-organelle signalling appears to be  
 20 responsible for the MAMP and effector associated transcriptional  
 21 repression of NECGs.

## 22 Discussion

23 We provide new insights into mechanisms underpinning plant innate  
 24 immunity and phytobacterial virulence strategies. Using virulent  
 25 DC3000 and a T3SS deficient DC3000/*hrpA* mutant we were able to  
 26 examine initial events in MTI and suppression of MTI. We show  
 27 that the chloroplast plays an early and important central role in inte-  
 28 grating disease and defence signals. MAMP recognition leads to rapid  
 29 transcriptional reprogramming of chloroplast encoded transcripts.  
 30 Within 3 hpi, virulent DC3000 bacteria modify the NECG transcripts  
 31 and deliver a subset of effectors into the chloroplast. Thus the  
 32 DC3000 virulence strategy acts both transcriptionally and post-trans-  
 33 criptionally to target the chloroplast, resulting in a rapid, non-stoma-  
 34 tal inhibition of photosynthesis in a T3E-dependent manner.  
 35 Chloroplast-targeted effectors collaborate to destabilize PSII and con-  
 36 sequent inhibition of photosynthetic electron transport decreases the  
 37 MAMP-induced ROS production we observed 5–6 hpi. Pathogen-  
 38 induced ABA contributes significantly to suppression of immunity.  
 39 PSII suppression can be mimicked by exogenous application of  
 40 ABA, or attenuated by prior activation of innate immune receptors  
 41 by MAMPs. Rational engineering of intervention strategies to  
 42 protect chloroplasts from bacterial effectors may well provide a  
 43 novel approach to broad-spectrum resistance against bacterial patho-  
 44 gens. If, as seems probable, key non-bacterial crop pathogens adopt  
 45 similar virulence strategies, then chloroplast intervention provides  
 46 considerable scope for restricting crop losses and simultaneously  
 47 improving productivity.

## 48 Methods

49 **Arabidopsis growth conditions.** *Arabidopsis thaliana* wild-type and mutant seed  
 50 were sown in a sieved compost mix (Levingston's F2 compost + sand (LEV206):  
 51 vermiculite (medium grade) mixed in a 6:1 ratio). Plants were grown in a controlled  
 52 environment growth chamber under a 10 h day (23 °C; 120  $\mu\text{mol m}^{-2} \text{s}^{-1}$ ) and  
 53 14 h night (20 °C) regime with relative humidity set to 65%. Plants were grown  
 54 for 4–5 weeks prior to use.

55 **Bacterial growth, maintenance and inoculation.** *Pseudomonas syringae* strains  
 56 were grown on solidified Kings B media containing appropriate antibiotics as  
 57 described<sup>8</sup>. *Xanthomonas campestris* strains were grown on Kings B without  
 58 antibiotics. For inoculation, overnight cultures were grown with shaking (200 rpm)  
 59 at 28 °C. Cells were harvested (2,000 g  $\times$  8 min), washed and resuspended in 10 mM  
 60  $\text{MgCl}_2$ . Cell density was adjusted to  $\text{OD}_{600}$  0.15 ( $\sim 0.75 \times 10^8$  colony forming  
 61 units (cfu)  $\text{ml}^{-1}$ ) for fluorescence and luciferase imaging or high inoculum growth  
 62 curves, or  $\text{OD}_{600}$  0.0002 for low inoculum growth assays. All growth curves were  
 63 repeated at least twice. All fluorescence and luciferase imaging experiments were  
 64 performed at least four times.

65 **Microarray data.** RNA was extracted at the appropriate time point from a single  
 66 challenged day 8 leaf and samples were cleaned up using a Qiagen RNeasy Plant

mini kit according to the manufacturer's instructions. Samples were hybridized to 67  
 CATMA arrays<sup>51</sup> and data processed exactly as described<sup>52</sup>. Data comprise 68  
 means from four single leaf biological replicates and two technical replicates per 69  
 time point and are deposited at GEO (Gene Expression Omnibus) under the 70  
 accession number GSE56094. The 32,578 CATMA probes were mapped to 25,115 71  
 unique AGI identifiers using the TAIR 9 release. The NECGs were derived as 72  
 follows: the TAIR GO.Slim annotations for 'Chloroplast' (accessed 19 February 73  
 2013) were used to identify 3,678 genes represented by the CATMA probes. NECG 74  
 expression data for Fig. 1 were generated using the Bioconductor package LIMMA 75  
 (Linear Models for Microarray Data) applying a *P* value cut-off of 0.05 and FDR 76  
 correction using the Benjamini–Hochberg method and annotations derived from 77  
 the TAIR9 release. 78

**Chlorophyll fluorescence imaging.** Photosystem II chlorophyll fluorescence 79  
 imaging of Arabidopsis rosettes was performed with a CF Imager (Technologica Ltd, 80  
 Colchester, UK). Plants were placed in the chamber for 40 min post-inoculation 81  
 and then dark adapted for 20 min. This was followed by a saturating light pulse 82  
 (6,349  $\mu\text{mol m}^{-2} \text{s}^{-1}$  for 0.8 s) to maximum obtain dark-adapted fluorescence (*Fm*). 83  
 Actinic light (120  $\mu\text{mol m}^{-2} \text{s}^{-1}$  – the same as plant growth light intensity) was then 84  
 applied for 15 min, followed by a saturating pulse to obtain maximum light adapted 85  
 fluorescence (*Fm'*). The plants were then left for a further 24 min in actinic light 86  
 before returning to the dark for 20 min. At this point the cycle of measurements 87  
 (59 min duration) was repeated 23 times. *Fm*, *Fm'* and *Fo* (minimal fluorescence 88  
 with fully oxidized PSII centres) were used to calculate chlorophyll fluorescence 89  
 parameters related to photosystem II photochemistry: *Fv/Fm* (maximum dark- 90  
 adapted quantum efficiency); maximum light adapted quantum efficiency (*Fv'/* 91  
*Fm'*); operating quantum efficiency (*Fq'/Fm'*); fraction of open PSII centres (qL) and 92  
 NPQ. The values were calculated as described by Baker<sup>13</sup>. The temperature during 93  
 measurements was 20 °C. 94

**Photosynthetic measurements.** Photosynthetic gas exchange measurements were 95  
 made using a portable open gas analysis system (CIRAS1, PP Systems, Amesbury, 96  
 Massachusetts, USA). The analyser was calibrated before use for  $\text{CO}_2$ , using a 97  
 standard gas ( $\pm 2.5\%$  tolerance) (BOC, UK) and for  $\text{H}_2\text{O}$  using a dew point generator 98  
 (LI-610, Li-Cor). The response of assimilation (*A*) rate to intercellular  $\text{CO}_2$  99  
 concentration (*C<sub>i</sub>*) was measured on whole leaves at a saturating photosynthetic 100  
 photon flux density (PPFD) of  $\sim 600 \mu\text{mol m}^{-2} \text{s}^{-1}$ . Leaves were initially stabilized in 101  
 the cuvette at ambient  $\text{CO}_2$  concentration (*C<sub>a</sub>*) of 400  $\mu\text{mol mol}^{-1}$ , leaf temperature 102  
 was maintained at  $23 \pm 2$  °C and vapour pressure deficit was  $\sim 1$  kPa. Following 103  
 stabilization *C<sub>a</sub>* was decreased to 300, 200, 100 and 75  $\mu\text{mol mol}^{-1}$  before returning 104  
 to the initial concentration. This was followed by an increase to 550, 700, 1,000 and 105  
 1,200  $\mu\text{mol mol}^{-1}$ . Readings were recorded when  $\text{CO}_2$  assimilation (*A*) had 106  
 stabilized to the new *C<sub>a</sub>* conditions (after about 2 min). The maximum velocity of 107  
 Rubisco for carboxylation (*V<sub>max</sub>*), the maximum rate of electron transport demand 108  
 for RuBP regeneration (*J<sub>max</sub>*), and respiration rate (*R<sub>d</sub>*) were derived by curve fitting 109  
 as described<sup>53</sup>. 110

The response of assimilation (*A*) rate to changing PPFD was measured using the 111  
 same open system immediately following the *A/C<sub>i</sub>* curves described above. Leaves 112  
 were initially stabilized at saturating irradiance ( $\sim 600 \mu\text{mol m}^{-2} \text{s}^{-1}$ ) and current 113  
 ambient  $\text{CO}_2$  concentration (400  $\mu\text{mol m}^{-2} \text{s}^{-1}$ ), after which PPFD was reduced in a 114  
 stepwise manner to 0  $\mu\text{mol m}^{-2} \text{s}^{-1}$ . Readings were recorded when  $\text{CO}_2$  assimilation 115  
 (*A*) had stabilized to the new PPFD levels (after about 1 min). The quantum 116  
 efficiency was determined from the linear slope of the curve at low PPFDs (between 117  
 0 and 100  $\mu\text{mol m}^{-2} \text{s}^{-1}$ ), while *A<sub>sat</sub>* was determined as the maximum light saturated 118  
 rate of *A*. 119

**Confocal microscopy.** Plants were challenged as described above. Following 120  
 treatment (2–3 hpi), leaves were detached and floated, adaxial surface upwards, in a 121  
 solution of 10 mM  $\text{MgCl}_2$  containing 10  $\mu\text{M}$  2',7'-dichlorodihydrofluorescein 122  
 diacetate ( $\text{H}_2\text{DCF-DA}$ ; Enzo) for at least 1 h, then washed for 20 min before 123  
 imaging. Pretreatment with ABA was as described<sup>17</sup>. DCMU (3-(3,4- 124  
 dichlorophenyl)-1,1-dimethylurea; Sigma) was co-infiltrated with bacteria at a 125  
 concentration of 10  $\mu\text{M}$ . Samples were mounted in perfluorodecalin<sup>54</sup> and images 126  
 were captured on a Leica SP8 using a 40 $\times$  oil immersion lens. Argon laser excitation 127  
 at 488 nm, and an emission window of 512–527 nm was used to capture the 128  
 dichlorofluorescein (DCF) signal. Chloroplast fluorescence was measured at 129  
 659–679 nm. 130

**In vivo chemiluminescence imaging.** *FRK1-LUC* plants (4–5 weeks old) were 131  
 sprayed with 1 mM D-luciferin (Sigma) in 0.01% v/v Triton X-100 and incubated in 132  
 the dark for 30 min. Sprayed plants were treated accordingly, placed in a dark box 133  
 and luciferase images acquired in a dark box at room temperature using a 134  
 Hamamatsu ORCAII ER CCD camera with a 35 mm f2.8 Nikkor lens. Photons were 135  
 counted every 5 min at 2  $\times$  2 binning mode using Wasabi imaging software 136  
 (Hamamatsu Photonics). 137

**Exploring common suppression patterns of NECGs in publically available 138**  
**microarray datasets.** Affymetrix gene chip data was obtained from NCBI GEO 139  
 (http://www.ncbi.nlm.nih.gov/geo/) or from NASCARRAYS (http://affymetrix. 140  
 arabidopsis.info) for the following experiments: NASCARRAYS59, 141  
 NASCARRAYS120, NASCARRAYS414, GSE10876, GSE49596, GSE10812, 142



1 GSE5726, GSE12887 and GSE5770. RMA normalization was performed using the  
2 Bioconductor package affy; replicates were averaged and the log<sub>2</sub> ratios were  
3 calculated between treatment and mock or wild-type and mutant. Transcript data  
4 was available for 3,445 NECG probe sets, these were filtered to 2,676 probe sets  
5 which exhibited expression changes greater than 1.5 fold in at least one treatment.  
6 Complete linkage hierarchical clustering was carried out using CLUSTER and  
7 visualized using TREEVIEW.

8 **Generation of flagellin induced receptor kinase promoter-luciferase plants.** The  
9 firefly luciferase coding sequence was removed from pGL4-11 (Promega; GenBank  
10 accession AF234298) by FseI digestion, T4 DNA polymerase treatment followed by  
11 KpnI digestion. This fragment was ligated into pCambia1302 digested with KpnI  
12 and PmlI to generate pCAMBIA-LUC2P. Amplification of the *FRK1* (At2g19190)  
13 promoter with *FRK1* KpnI 5'-TTGGTACCGGACAACCACGGAAGTTATTAGC-  
14 3' and *FRK1* NcoI 5'-GACCCGGGTACCGAGAAGTTGG-3' primers generated a  
15 2,152 bp fragment that was digested with KpnI and NcoI and ligated into the  
16 complementary sites of the pCAMBIA-LUC2P derivative. Sequence validated  
17 constructs were transformed into *Agrobacterium tumefaciens* (GV3101) used to  
18 transform *Arabidopsis thaliana* ecotype Col-0 by the floral dip method. Transgenic  
19 lines were selected on gentamycin and homozygous lines isolated.

20 **Effector import into chloroplasts.** Effector N-termini (about 150 aa), fused to GFP,  
21 were radiolabelled by *in vitro* expression (TNT T7 reticulocyte lysate kit, Promega).  
22 Import into isolated pea chloroplasts<sup>35</sup> equivalent to 20 µg of chlorophyll was  
23 allowed for 1 h at 30 °C. Subsequently, chloroplasts were re-purified and half of the  
24 reaction was incubated with 2 µg thermolysin for 20 min on ice to digest non-  
25 imported proteins. Reaction products were separated by SDS-PAGE and visualized  
26 on X-ray films.

27 Received 30 October 2014; accepted 24 April 2015;  
28 published online XX XX 2015

## 29 References

30 1. Bohm, H., Albert, I., Fan, L., Reinhard, A. & Nurnberger, T. Immune receptor  
31 complexes at the plant cell surface. *Curr. Opin. Plant Biol.* **20C**, 47–54 (2014).  
32 2. Macho, A. P. & Zipfel, C. Plant PRRs and the activation of innate immune  
33 signaling. *Mol. Cell* **54**, 263–272 (2014).  
34 3. Shapiguzov, A., Vainonen, J. P., Wrzaczek, M. & Kangasjarvi, J. ROS-talk – how  
35 the apoplast, the chloroplast, and the nucleus get the message through. *Front.*  
36 *Plant Sci.* **3**, 292 (2012).  
37 4. Galvez-Valdivieso, G. & Mullineaux, P. M. The role of reactive oxygen species in  
38 signalling from chloroplasts to the nucleus. *Physiol. Planta* **138**, 430–439 (2010).  
39 5. Robert-Seilaniantz, A., Grant, M. & Jones, J. D. Hormone crosstalk in plant  
40 disease and defense: more than just jasmonate-salicylate antagonism. *Annu. Rev.*  
41 *Phytopathol.* **49**, 317–343 (2011).  
42 6. Trotta, A., Rahikainen, M., Konert, G., Finazzi, G. & Kangasjarvi, S. Signalling  
43 crosstalk in light stress and immune reactions in plants. *Phil. Trans. R. Soc. B*  
44 **369**, 20130235 (2014).  
45 7. Cunnac, S., Lindeberg, M. & Collmer, A. *Pseudomonas syringae* type III  
46 secretion system effectors: repertoires in search of functions. *Curr. Opin.*  
47 *Microbiol.* **12**, 53–60 (2009).  
48 8. Truman, W., Zabala, M. D. T. & Grant, M. Type III effectors orchestrate a  
49 complex interplay between transcriptional networks to modify basal defense  
50 responses during pathogenesis and resistance. *Plant J.* **46**, 14–33 (2006).  
51 9. Smyth, G. K., Michaud, J. & Scott, H. S. Use of within-array replicate spots  
52 for assessing differential expression in microarray experiments. *Bioinformatics*  
53 **21**, 2067–2075 (2005).  
54 10. Zipfel, C. *et al.* Bacterial disease resistance in *Arabidopsis* through flagellin  
55 perception. *Nature* **428**, 764–767 (2004).  
56 11. Windram, O. *et al.* *Arabidopsis* defense against *Botrytis cinerea*: chronology and  
57 regulation deciphered by high-resolution temporal transcriptomic analysis.  
58 *Plant Cell* **24**, 3530–3557 (2012).  
59 12. Grant, M. *et al.* The RPM1 plant disease resistance gene facilitates a rapid and  
60 sustained increase in cytosolic calcium that is necessary for the oxidative burst  
61 and hypersensitive cell death. *Plant J.* **23**, 441–450 (2000).  
62 13. Baker, N. R. Chlorophyll fluorescence: a probe of photosynthesis *in vivo*. *Annu.*  
63 *Rev. Plant Biol.* **59**, 89–113 (2008).  
64 14. Muller, P., Li, X. P. & Niyogi, K. K. Non-photochemical quenching. A response  
65 to excess light energy. *Plant Physiol.* **125**, 1558–1566 (2001).  
66 15. Zheng, X. Y. *et al.* Coronatine promotes *Pseudomonas syringae* virulence in  
67 plants by activating a signaling cascade that inhibits salicylic acid accumulation.  
68 *Cell Host Microbe* **11**, 587–596 (2012).  
69 16. Gohre, V., Jones, A. M., Sklenar, J., Robatzek, S. & Weber, A. P. Molecular  
70 crosstalk between PAMP-triggered immunity and photosynthesis. *Mol. Plant*  
71 *Microbe Interact.* **25**, 1083–1092 (2012).  
72 17. de Torres Zabala, M., Bennett, M. H., Truman, W. H. & Grant, M. R.  
73 Antagonism between salicylic acid and abscisic acid reflects early host-pathogen  
74 conflict and moulds plant defence responses. *Plant J* (2009).

18. Debener, T., Lehnackers, H., Arnold, M. & Dangl, J. L. Identification and  
molecular mapping of a single *Arabidopsis thaliana* locus determining resistance  
to a phytopathogenic *Pseudomonas syringae* isolate. *Plant J.* **1**, 289–302 (1991).  
19. Taylor, J. D., Conway, J., Roberts, S. J., Astley, D. & Vicente, J. G. Sources and  
origin of resistance to *Xanthomonas campestris* pv. *campestris* in brassica  
genomes. *Phytopathology* **92**, 105–111 (2002).  
20. Kvitko, B. H. *et al.* Deletions in the repertoire of *Pseudomonas syringae* pv.  
tomato DC3000 type III secretion effector genes reveal functional overlap among  
effectors. *PLoS Pathogens* **5**, e1000388 (2009).  
21. Cunnac, S. *et al.* Genetic disassembly and combinatorial reassembly identify a  
minimal functional repertoire of type III effectors in *Pseudomonas syringae*.  
*Proc. Natl Acad. Sci. USA* **108**, 2975–2980 (2011).  
22. Gomez-Gomez, L. & Boller, T. Flagellin perception: a paradigm for innate  
immunity. *Trends Plant Sci.* **7**, 251–256 (2002).  
23. Kunze, G. *et al.* The N terminus of bacterial elongation factor Tu elicits innate  
immunity in *Arabidopsis* plants. *Plant Cell* **16**, 3496–3507 (2004).  
24. Wiermer, M., Feys, B. J. & Parker, J. E. Plant immunity: the EDS1 regulatory  
node. *Curr. Opin. Plant Biol.* **8**, 383–389 (2005).  
25. de Torres-Zabala, M. *et al.* *Pseudomonas syringae* pv. tomato hijacks the  
*Arabidopsis* abscisic acid signalling pathway to cause disease. *EMBO J.*  
**26**, 1434–1443 (2007).  
26. Rubio, S. *et al.* Triple loss of function of protein phosphatases type 2C leads  
to partial constitutive response to endogenous abscisic acid. *Plant Physiol.*  
**150**, 1345–1355 (2009).  
27. Asai, T. *et al.* MAP kinase signalling cascade in *Arabidopsis* innate immunity.  
*Nature* **415**, 977–983 (2002).  
28. Figueiredo, J. F. *et al.* *Agrobacterium*-mediated transient expression in citrus  
leaves: a rapid tool for gene expression and functional gene assay. *Plant Cell Rep.*  
**30**, 1339–1345 (2011).  
29. Jelenska, J. *et al.* A J domain virulence effector of *Pseudomonas syringae*  
remodels host chloroplasts and suppresses defenses. *Curr. Biol.* **17**,  
499–508 (2007).  
30. Li, G. *et al.* Distinct *Pseudomonas* type-III effectors use a cleavable transit  
peptide to target chloroplasts. *Plant J.* **77**, 310–321 (2014).  
31. Rodriguez-Herva, J. J. *et al.* A bacterial cysteine protease effector protein  
interferes with photosynthesis to suppress plant innate immune responses.  
*Cell. Microbiol.* **14**, 669–681 (2012).  
32. Jelenska, J., van Hal, J. A. & Greenberg, J. T. *Pseudomonas syringae* hijacks plant  
stress chaperone machinery for virulence. *Proc. Natl Acad. Sci. USA* **107**,  
13177–13182 (2010).  
33. Emanuelsson, O., Brunak, S., von Heijne, G. & Nielsen, H. Locating proteins  
in the cell using TargetP, SignalP and related tools. *Nature Protocols* **2**,  
953–971 (2007).  
34. Mukhtar, M. S. *et al.* Independently evolved virulence effectors converge  
onto hubs in a plant immune system network. *Science* **333**, 596–601 (2011).  
35. Waegemann, K. & Soll, J. Characterization of the protein import apparatus  
in isolated outer envelopes of chloroplasts. *Plant J.* **1**, 149–158 (1991).  
36. Macho, A. P. *et al.* Genetic analysis of the individual contribution to virulence  
of the type III effector inventory of *Pseudomonas syringae* pv. *phaseolicola*.  
*PLoS One* **7**, e35871 (2012).  
37. Fu, Z. Q. *et al.* A type III effector ADP-ribosylates RNA-binding proteins and  
quells plant immunity. *Nature* **447**, 284–288 (2007).  
38. Baba, K., Nakano, T., Yamagishi, K. & Yoshida, S. Involvement of a nuclear-  
encoded basic helix-loop-helix protein in transcription of the light-responsive  
promoter of *psbD*. *Plant Physiol.* **125**, 595–603 (2001).  
39. Shi, L. X. & Schroder, W. P. The low molecular mass subunits of the  
photosynthetic supracomplex, photosystem II. *Biochim. Biophys. Acta*  
**1608**, 75–96 (2004).  
40. Ikeuchi, M. *et al.* Cloning of the *psbK* gene from *Synechocystis* sp. PCC 6803  
and characterization of photosystem II in mutants lacking PSII-K. *J. Biol. Chem.*  
**266**, 11111–11115 (1991).  
41. Wessling, R. *et al.* Convergent targeting of a common host protein-network  
by pathogen effectors from three kingdoms of life. *Cell Host Microbe* **16**,  
364–375 (2014).  
42. Torres, M. A., Jones, J. D. & Dangl, J. L. Reactive oxygen species signaling in  
response to pathogens. *Plant Physiol.* **141**, 373–378 (2006).  
43. Mitchell, K., Brown, I., Knox, P. & Mansfield, J. The role of cell wall-based  
defences in the early restriction of non-pathogenic *hrp* mutant bacteria in  
*Arabidopsis*. *Phytochemistry* (2014).  
44. Hempel, S. L., Buettner, G. R., O'Malley, Y. Q., Wessels, D. A. & Flaherty, D. M. 144  
Dihydrofluorescein diacetate is superior for detecting intracellular oxidants:  
comparison with 2',7'-dichlorodihydrofluorescein diacetate, 5-(and 6)-carboxy-  
2',7'-dichlorodihydrofluorescein diacetate, and dihydrorhodamine 123. *Free*  
*Rad. Biol. Med.* **27**, 146–159 (1999).  
45. Halliwell, B. & Whiteman, M. Measuring reactive species and oxidative damage  
in vivo and in cell culture: how should you do it and what do the results mean?  
*Brit. J. Pharmacol.* **142**, 231–255 (2004).  
46. Mubarakshina, M. M. *et al.* Production and diffusion of chloroplastic H<sub>2</sub>O<sub>2</sub> and  
its implication to signalling. *J. Exp. Bot.* **61**, 3577–3587 (2010).  
153

- 1 47. Flors, C. *et al.* Imaging the production of singlet oxygen in vivo using a  
2 new fluorescent sensor, Singlet Oxygen Sensor Green. *J. Exp. Bot.* **57**,  
3 1725–1734 (2006).
- 4 48. Krieger-Liszkay, A. Singlet oxygen production in photosynthesis. *J. Exp. Botany*  
5 **56**, 337–346 (2005).
- 6 49. Lee, K. P., Kim, C., Landgraf, F. & Apel, K. EXECUTER1- and EXECUTER2-  
7 dependent transfer of stress-related signals from the plastid to the nucleus of  
8 *Arabidopsis thaliana*. *Proc. Natl Acad. Sci. USA* **104**, 10270–10275 (2007).
- 9 50. Larkin, R. M. Influence of plastids on light signalling and development.  
10 *Phil. Trans. R. Soc. B* **369**, 20130232 (2014).
- 11 51. Allemeersch, J. *et al.* Benchmarking the CATMA microarray. A novel tool for  
12 *Arabidopsis* transcriptome analysis. *Plant Physiol.* **137**, 588–601 (2005).
- 13 52. Breeze, E. *et al.* High-resolution temporal profiling of transcripts during  
14 *Arabidopsis* leaf senescence reveals a distinct chronology of processes and  
15 regulation. *Plant Cell* **23**, 873–894 (2011).
- 16 53. Sharkey, T. D., Bernacchi, C. J., Farquhar, G. D. & Singsaas, E. L. Fitting  
17 photosynthetic carbon dioxide response curves for C(3) leaves. *Plant Cell*  
18 *Environ.* **30**, 1035–1040 (2007).
- 19 54. Littlejohn, G. R., Gouveia, J. D., Edner, C., Smirnov, N. & Love, J.  
20 Perfluorodecalin enhances in vivo confocal microscopy resolution of  
21 *Arabidopsis thaliana* mesophyll. *New Phytol.* **186**, 1018–1025 (2010).

## Acknowledgements

This work was funded by BBSRC grants BB/E010334/1 to M.G. and BB/F005903/1 to M.G. and N.S. M.T. and D.L. thank Ralph Bock and the Max Planck Society (MPG) for their support. We are indebted to members of the PRESTA consortium for their efforts in generating the microarray data. We thank Jean Greenberg for the Pma4326 *hop11* strain and Emilia Lopez-Solanilla for the HopN1 derivatives. We are indebted to Krzysztof Polanski for generating the images for Fig. 1b.

## Author contributions

M.G., M.d.T., J.M., M.T. and N.S. conceived the experiments, M.T., D.L., L.D. and B.B. undertook the chloroplast localization and effector predictions, S.J., T.B. and D.S. the bioinformatics, T.L., N.S. the photosynthesis experiments, G.L. the microscopy and M.d.T. and W.T. contributed to the remainder of the experimental work. M.d.T., M.G., N.S., J.M. and M.T. wrote the manuscript.

## Additional information

Supplementary information is available online. Reprints and permissions information is available online at [www.nature.com/reprints](http://www.nature.com/reprints). Correspondence and requests for materials should be addressed to M.G.

## Competing interests

The authors declare no competing financial interests.

22  
23  
24  
25  
26  
27  
28  
29  
30  
31  
32  
33  
34  
35  
36  
37  
38  
39  
40

Q5

Journal: NPLANTS

Article ID: nplants.2014.74

Article Title: Chloroplasts play a central role in plant defence and are targeted by pathogen effectors

Author(s): Marta de Torres-Zabala *et al.*

Query no.	Queries	Response
Q1	Please check the use of italics for variables throughout and correct if necessary.	
Q2	Please check that all highlighted text is correct and amend if necessary.	
Q3	Please provide volume and page numbers for reference 17.	
Q4	Please provide volume and page numbers for reference 43.	
Q5	Please check Additional information section is correct	